COMMUNICATION

Piezophototronic-Effect-Enhanced Electrically Pumped Lasing

Xun Yang, Lin Dong, Chongxin Shan,* Junlu Sun, Nan Zhang, Shuangpeng Wang, Mingming Jiang, Binghui Li, Xiuhua Xie, and Dezhen Shen**

Electrically pumped UV semiconductor lasers have significant potential applications in information storage,[1] communications,[2] photonics,[3,4] medical diagnostics and therapeutics,[5–7] etc. ZnO, as a direct wide band gap semiconductor (3.37 eV) with relatively large exciton binding energy (60 meV), is considered a promising material for efficient excitonic lasing.[8–10] Meanwhile, ZnO nanostructures usually exhibit merits of high crystalline and optical quality,[8,11] which favors the low threshold lasing. Quite a few attempts have been made to realize ZnO-based electrically pumped lasers;[7–9,12] however, effective carrier injection and recombination in ZnO remains one of the major obstacles for practical applications, and the performance of the ZnO lasers needs still much improvements.

In recent years, piezotronic and piezophototronic effects have attracted increasing attention to tune the carrier transportation and recombination of various semiconductor devices. As for wurtzite ZnO, such effects stem from the noncentral symmetry of the crystalline structure. Without strain, the cations and anions in the wurtzite crystal are tetrahedrally coordinated and the centers of the cations and anions overlap with each other. When certain strain is applied along the *c*-axis of ZnO, the centers of the cations and anions separate, leading to the electric dipole moments which will create a piezopotential within the crystal. The piezopotential can be used to improve the performance of optoelectronic devices by tuning the carrier transportation, recombination, or separation.[13] ZnO has the highest piezoelectric tensor among the tetrahedrally bonded semiconductors,[14] which makes it a technologically important material for many applications requiring a large electromechanical coupling coefficient. If the two remarkable properties of ZnO, i.e., large exciton binding energy and high piezoelectric tensor, can be utilized simultaneously, significant improvements may be achieved because of the piezotronic and/or piezophototronic effect.[15,16] The piezopotential has been utilized to develop piezotronic devices from ZnO-based materials, such as nanogenerators,[17,18] piezotronic diodes,[19,20] and field effect transistors,[21,22] as well as to improve the performance of ZnO optoelectronic devices such as solar cells,[23,24] photodetectors,[25,26] and light-emitting devices (LEDs).[27,28] But so far, no such report can be found for electrically pumped lasing.

In this work, we utilize piezophototronic effect to enhance the performance of electrically pumped lasers for the first time, and the lasers were realized in *p*-GaN/MgO/ZnO nanowire (NW) structured laser diode (LD). The threshold voltage of the lasers has been reduced from 48 to 20 V by applying a pressure of 16.0 kPa on the device, and the emission efficiency and injection current at a fixed applied voltage of 50 V have been enhanced by a factor of 3.95 and 1.25, respectively. Meanwhile, the output power has been enhanced by 496%. The improvements of the lasing characteristics can be attributed to the improved current injection and enhanced emission efficiency via piezophototronic effect. The results may provide a route to improve the performance of laser devices based on piezoelectric semiconductors.

Figure 1a shows the fabrication process of LD-a. The role of the MgO layer has been detailed in our previous work: by hindering the electrons in the *n*-ZnO from entering into the *p*-GaN, appropriate insulating buffer layer may help to enhance the emission from ZnO.[29,30] Moreover, the MgO thin layer can protect *p*-GaN from being oxidized during the growth of the ZnO NWs.[31,32] Scanning electron microscopy (SEM) images (Figure 1b,c) show that the ZnO NWs are grown vertically on the MgO/*p*-GaN structure with an average length and diameter of 1.3 μm and 25 nm, respectively. Transmission electron microscopy (TEM) was used to determine the polar direction of the ZnO NWs, as illustrated in **Figure 2**. Figure 2a,b shows the schematic atomic structures of wurtzite ZnO and the unit cells viewed along the [110] projection. Figure 2c shows the simulated TEM images of the ZnO NWs with different polar directions along the [110] projection by QSTEM software. The simulated TEM images show distinct dots with a tail, and the position of the tail depends on the +*c* or –*c*-axis direction of the NWs. This distinction in TEM images provides a way to determine the ZnO NWs polar direction directly. Figure 2d,e shows the TEM image of the ZnO NWs and the corresponding selected area electron diffraction (SAED) pattern, clear dotted pattern is visible from the figure, indicating the high crystalline quality of the NWs. Figure 2f shows the high-resolution TEM

X. Yang, Prof. L. Dong, Prof. C. Shan, J. Sun
School of Physics and Engineering
Zhengzhou University
Zhengzhou 450001, China
E-mail: ldong@zzu.edu.cn
X. Yang, Prof. C. Shan, Dr. S. Wang, Dr. M. Jiang, B. Li, Dr. X. Xie, Prof. D. Shen
State Key Laboratory of Luminescence and Applications, Changchun Institute of Optics Fine Mechanics and Physics
Chinese Academy of Sciences
Changchun 130033, China
E-mail: shancx@ciomp.ac.cn; shendz@ciomp.ac.cn
X. Yang, N. Zhang
Chinese Academy of Sciences
Beijing 100049, China

DOI: 10.1002/adma.201602832

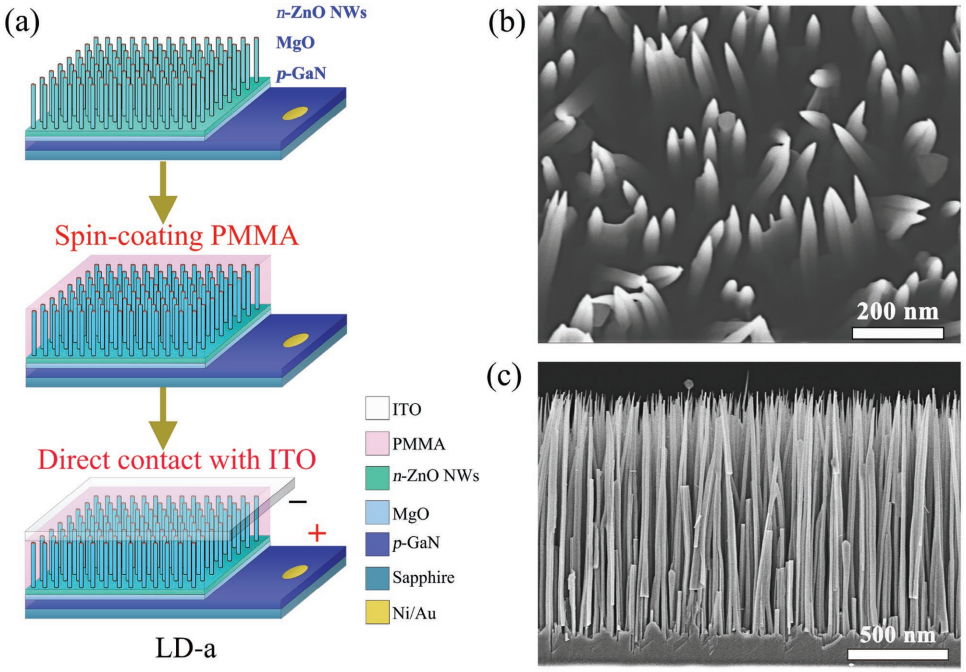

Figure 1. Fabrication of LD-a. a) Fabrication process of LD-a. A 10 nm MgO film was grown on *p*-GaN by MBE, then ZnO NWs were grown on the MgO/*p*-GaN substrate using MOCVD. After spin-coating PMMA onto the ZnO NWs, a transparent ITO film was deposited on top of the ZnO NWs to form an electrode. Ni/Au electrodes were prepared on *p*-GaN by thermal evaporation method. b,c) The SEM images of the as-grown ZnO NWs arrays on the MgO/*p*-GaN film.

(HRTEM) image of an individual ZnO NW, which shows the same relative position of dots and tails with the simulated TEM image of the ZnO grown along the +*c*-axis direction shown in the inset of this figure. By comparing the simulated TEM image with the measured one, we confirm that the ZnO NWs in our case grow along the +*c*-axis direction. Figure 2g shows the simulated piezopotential distribution in an individual ZnO NW under strain by a finite-element analysis method (COMSOL). As wurtzite crystal has noncentral symmetric structure, relative displacement of Zn^{2+} and O^{2-} under strain along the *c*-axis will cause dipole moments, which add up to a macroscopic piezopotential between two ends of the ZnO NW. A typical piezopotential drop of 1.0 V is created under an external compressive force of 25 nN, with the –*c*-axis side positive.

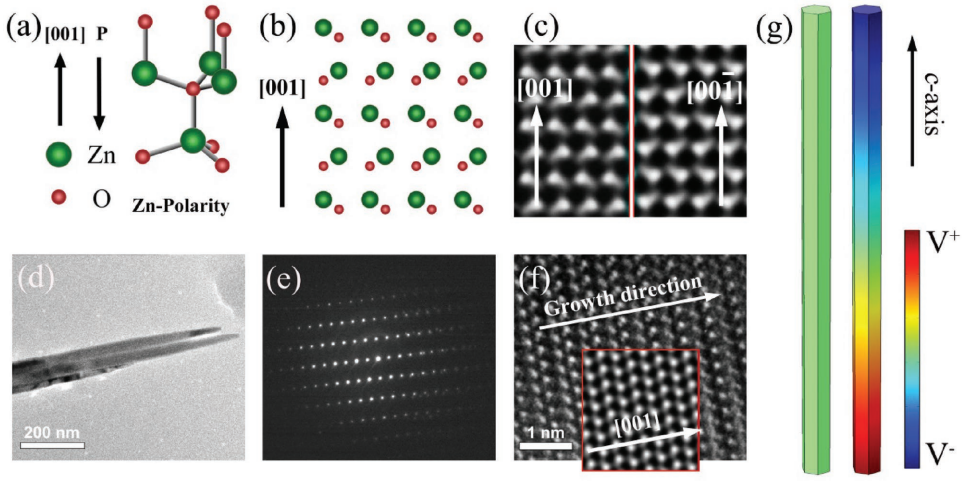

Figure 2. ZnO NWs orientation determination. a) Stick and ball representation of ZnO wurtzite crystal structure. b) ZnO unit cell viewed along the [110] direction. c) QSTEM simulated TEM images of the ZnO with different polar directions along the [110] projection. d,e) TEM image of a single ZnO NW and the corresponding SAED pattern. f) High-resolution TEM image of the ZnO NW showing its +*c*-axis growth direction compared with the simulated TEM image of the inset. g) Simulated piezopotential distributions in a single ZnO NW with and without pressure by a finite-element analysis method, and the diameter and length used for simulation are 25 nm and 1.3 µm, respectively. The electron density and mobility in the ZnO NW are 5×10^{16} cm^{-3} and 3 cm^2 V^{-1} s^{-1}, respectively.

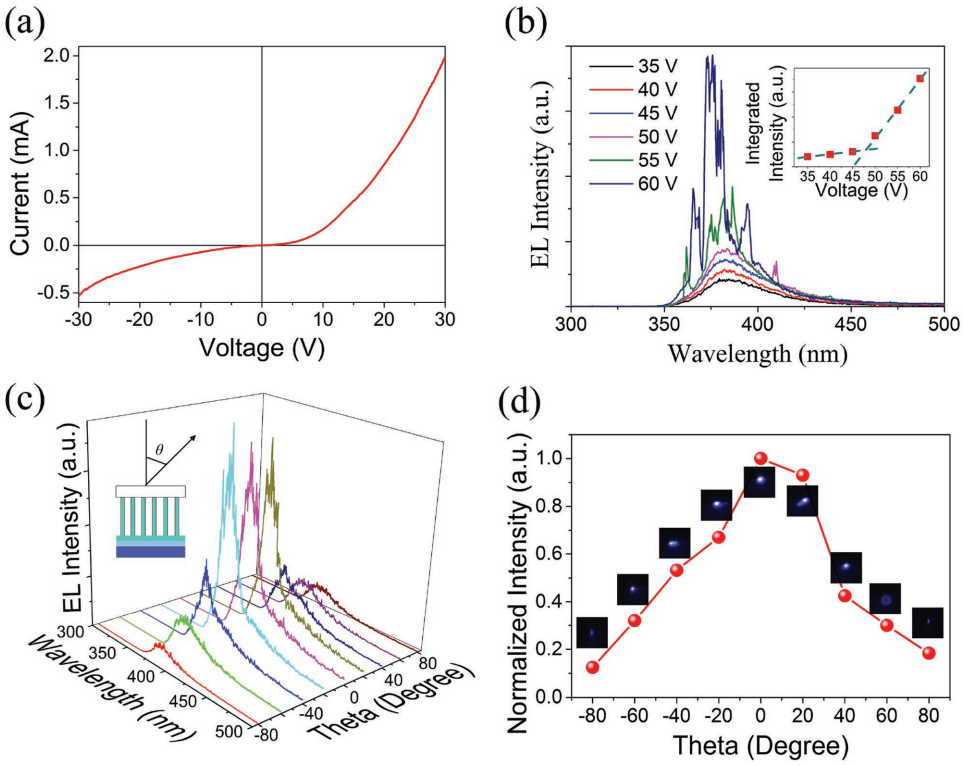

Figure 3. Characteristics of the as-fabricated LD-a. a) *I–V* curve of LD-a. b) EL spectra of LD-a as a function of applied bias, and the inset illustrates the integrated emission intensity versus applied bias. c) Angle-dependent EL spectra at a fixed bias of 50 V, the inset shows the schematic illustration of the measurement setup. d) The integrated emission intensity and optical images as a function of observation angle.

The current–voltage (*I–V*) curve of LD-a exhibits typical rectifying behavior with a turn-on voltage of around 5.5 V, as indicated in **Figure 3**a. Under forward bias, electroluminescence (EL) emission can be detected, as shown in Figure 3b. At low applied bias, only a broad emission at around 383 nm is observed, which can be attributed to the near band edge emission of ZnO. When the applied bias is increased to 50 V, sharp peaks emerge from the shoulder of the broad emission. As the applied voltage increases further, more sharp peaks appear. The integrated emission intensity exhibits a superlinear increase with the applied bias, as indicated in the inset of Figure 3b, which symbolizes that a lasing phenomenon has occurred.[33,34] The full width at half maximum of the peaks is around 0.8 nm. By linear fitting of the integrated intensity versus bias applied, the threshold voltage for lasing of about 48 V is obtained. Figure 3c shows the angle-dependent emission spectra of LD-a at a fixed bias of 50 V. The angle of theta has been defined as the observation angle between the detector and the normal of the sample surface, as shown in the inset of Figure 3c. Figure 3d shows the integrated intensity and optical images of the emission at different observation angles. It is obvious that the emission intensity reaches its maximum when the detector is perpendicular to the surface of the sample, and the intensity decreases gradually when the detector deviates from the normal of the sample. From the above EL data, one can see that electrically pumped lasing has been realized from the *p*-GaN/MgO/ZnO NWs structure. As no elaborate Fabry-Pérot (F-P) cavity has been introduced in the structure, the lasing should originate from random cavities formed among the ZnO NWs, note that the random lasing may have been modulated by the weak F-P cavity formed by the indium tin oxide (ITO) glass and substrate, and the detailed formation mechanism of the random laser can be found in literatures.[35–37] The realization of electrically pumped lasing lays a solid ground for the following piezophototronic study on the lasing.

To study the piezophototronic effect on the lasing characteristics of the *p*-GaN/MgO/ZnO NWs structure, the emission characteristics of the structure under pressure have been investigated, as indicated in **Figure 4**. Figure 4a shows the dependence of the output power of LD-a on the applied pressure at a fixed bias of 50 V. In this paper, the pressure is calculated by dividing the applied force by the overall contact area between the *p*-GaN layer and the ITO electrode for simplicity. The fill rate of the NWs is less than 5%, as estimated from the size (around 25 nm in diameter) and density (around 90 μm^{-2}) of the NWs. We also note that since the devices were formed by direct contact method, the contact uniformity is poor, only less than 1% area of the devices bear the pressure and take effect as estimated by dividing the emission area by the overall contact area, as shown in Figure S1 (Supporting Information). Thus the actual pressure on the working ZnO NW can be three or four orders of magnitude higher. The output power of the device increases gradually with the pressure, and an enhancement factor of 4.96 (from 6.8 to 33.7 nW) has been achieved by applying a pressure of 16.0 kPa on the device. The remarkable enhancement of the output power can also be identified

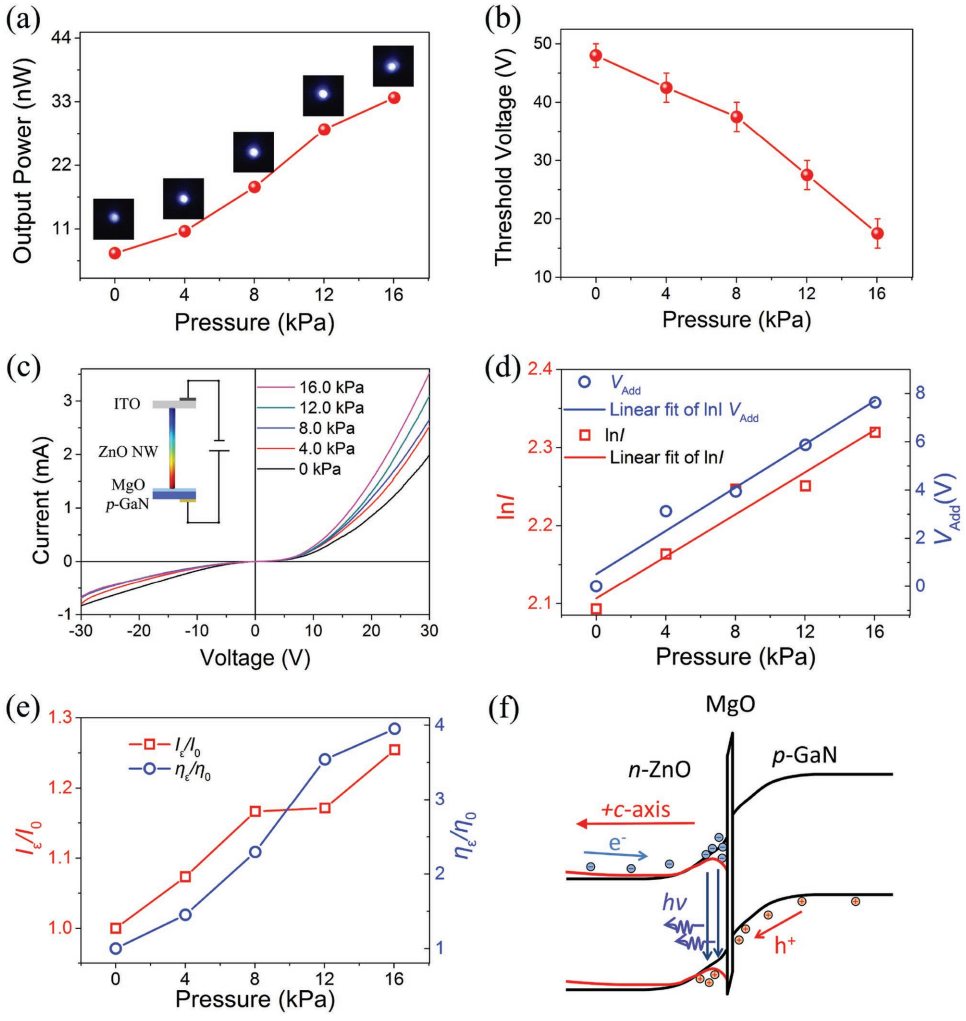

Figure 4. Performance improvements of LD-a by applying pressure. a) Output power enhancement and optical images at a fixed bias of 50 V as a function of pressure. b) Decrease of threshold voltage under different pressure. c) *I–V* curves as a function of pressure applied onto the structures, and the inset shows the direction of forward bias and piezopotential. d) Logarithm plot of current at a fixed bias of 30 V and the calculated additional external voltage (V_{Add}) as a function of applied pressure. e) Changes in relative injection current I_ε/I_0 and relative external efficiency η_ε/η_0 versus pressure. f) Schematic band diagram of the *p*-GaN/MgO/ZnO NWs before (black line) and after (red line) applying of pressure with *c*-axis of ZnO NWs pointing away from *p*-GaN.

from the optical images. The dependence of the threshold voltage of the lasing on the pressure applied has been derived, as indicated in Figure 4b. The threshold voltage of LD-a shows a monotonic reducing from 48 to 20 V with the increase of the applied pressure from 0 to 16.0 kPa, indicating that the pressure has great effect on the lasing threshold voltage of the *p*-GaN/MgO/ZnO NWs structure.

To explore the origin of the pressure-dependent lasing characteristics, the carrier transport and emission efficiency of the structure under pressure have been studied. Figure 4c shows *I–V* characteristics of LD-a under different applied pressure. The current increases with applied pressure under forward bias and decreases under reverse bias. The asymmetric change of *I–V* characteristics is mainly a result of the polarized piezopotential in the ZnO NWs because other factors caused by external pressure, such as band shifting, piezoresistance, or contact area variation, will induce symmetric changes of *I–V* characteristics, regardless of the direction of the bias.[26,38] It is reasonable to consider that the piezopotential exists mostly in the ZnO NWs because the strain occurs mainly on the ZnO NWs rather than on the dense GaN film.[39] According to the simulation, an additional positive piezopotential will be created at the interface of ZnO NW and MgO under compressive strain (Figure 2g). The piezopotential in the ZnO NWs may work together with the applied external bias as an additional positive bias (V_{Add}), as shown in inset of Figure 4c, which may reduce the depletion layer width.[25,40] So the current injection may be improved by the piezopotential, thus leading to the improved emission. The current of a *p–n* junction can be determined by[41]

$$I = I_s\left[\exp\left(\frac{V}{V_T}\right) - 1\right] \quad (1)$$

where I_s is the reverse saturation current and V_T is the thermal voltage. At large voltage (when $V \gg V_T$), $\exp(V/V_T) - 1 \sim \exp(V/V_T)$,

thus $\ln I = \ln I_s + V/V_T$. In consideration of the V_{Add}, $\ln I$ can be expressed as follows

$$\ln I = \ln I_s + \frac{V_{Add}}{V_T} + \frac{V}{V_T} \quad (2)$$

Because the piezopotential has a linear relationship with the applied pressure,[25,26,42] $\ln I$ at a fixed bias should change linearly with the pressure applied onto the NWs, as shown in Figure 4d (red line). Using linear fitting of the voltage with logarithm of current (between 25 and 30 V), one can estimate the equivalent V_{Add} under variant pressure. As shown in Figure 4d (blue line), the calculated V_{Add} shows linear changes with applied pressure. The calculated equivalent V_{Add} of LD-a under 16.0 kPa pressure is 7.6 V, which is distinctly larger than the pressure induced piezopotential in ZnO NWs. Thus, to improve the current injection and output power, only a small piezopotential in ZnO NWs is needed to influence the carrier transport.

Piezopotential also has a strong impact on emission efficiency due to the piezophototronic effect. External quantum efficiency (EQE), the ratio between the externally produced photo flux and the injected electron flux, can be expressed by the following formula[26]

$$\eta_\varepsilon = \frac{P}{I} \cdot \frac{e}{h\nu} \quad (3)$$

where P is the output power, I is the current, e is the electron charge, h is Planck constant, and ν is the frequency of the emitting light. Figure 4e shows the changes in relative injection current (I_ε/I_0) and relative external efficiency (η_ε/η_0) of LD-a at 50 V, as a function of applied pressure. The injection current and the emission efficiency have been enhanced by a factor of 1.25 and 3.95, respectively, under a pressure of 16.0 kPa. The change in relative injection current is much smaller than that of relative external efficiency, which indicates that the change of output power is mainly caused by the enhanced EQE due to the piezophototronic effect.

To understand the effect of the piezophototronic effect on the lasing characteristics of the *p*-GaN/MgO/ZnO NW structure, a schematic band diagram of the structure before (black line) and after (red line) applying pressure has been plotted, as shown in Figure 4f. In this structure, since the conduction band offset between the ZnO and MgO layer is as large as 3.55 eV, which forms a huge barrier that can confine electrons in the *n*-ZnO side when the structure is forward biased, while holes in the *p*-GaN layer can be injected into ZnO layer because of the much smaller barrier height (0.9 eV). Furthermore, because of the dielectric nature of the MgO layer, the voltage will be mainly applied onto this layer, thus the conduction band and valence band of the MgO layer will be bent greatly under forward bias, and the effective thickness of the barrier that hinders the injection of holes will be decreased significantly. Then the holes can be injected from the *p*-GaN side into the ZnO side and recombine radiatively with the electrons confined in the ZnO layer. The emitted photons will undergo strong scattering when they comes out of the ZnO since the refractive index of ZnO (2.45) is much larger than that of polymethyl

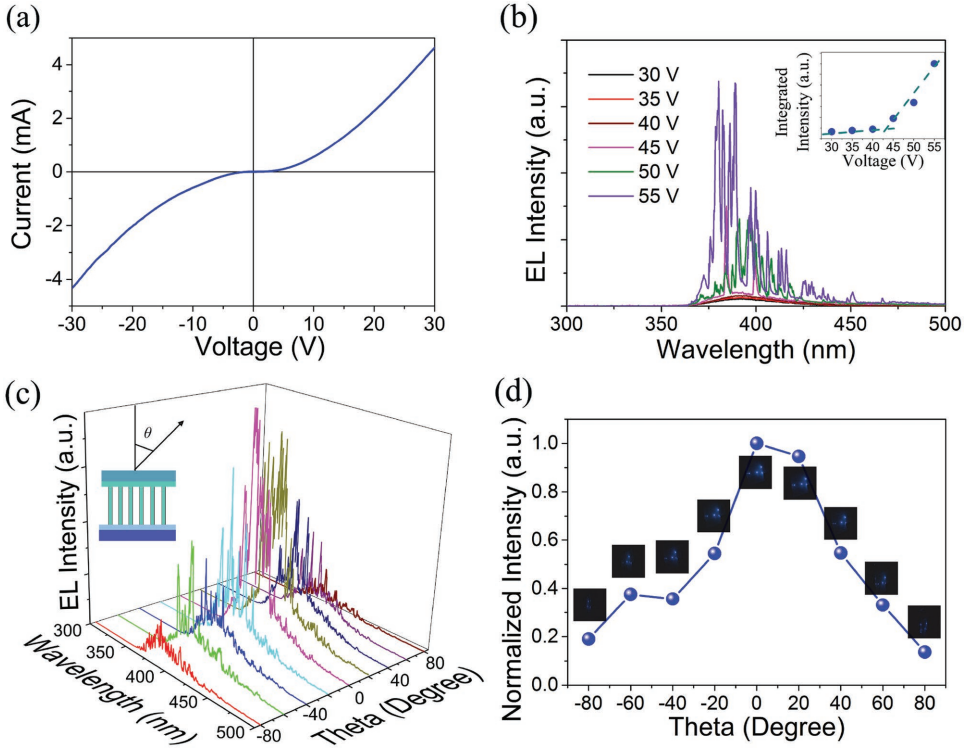

Figure 5. Characteristics of the as-fabricated LD-b. a) *I–V* curve. b) EL spectra of LD-b as a function of applied bias and the dependence of integrated emission intensity on applied bias is shown in the inset. c) Angle-dependent EL spectra at a fixed bias of 50 V, the inset shows the schematic illustration of the measurement setup. d) The integrated emission intensity and optical images versus observation angle.

methacrylate (PMMA) filling the interspace of the nanowires (1.49). The large surface of the nanowires provides an ideal arena for the scattering. In certain cases, the photons may return to its original site after several scattering processes, then closed loops will form. At larger injection current when the gain in the closed loops exceeds the loss, lasing will occur.[8,29] As demonstrated in Figure 2g, the +*c*-axis of the ZnO NWs is pointing away from the *p*-GaN side, so compressive strain will create a positive piezopotential in the ZnO NWs at the *p*–*n* junction region. The piezopotential creates a downward bent in the valence and conduction band of the ZnO. Electrons tend to be temporarily trapped and accumulated near the interface of ZnO and MgO by distortion in the band, which increases the recombination rate of electrons with injected holes, resulting in the enhanced emission efficiency.[25,26] The improved current injection and enhanced emission efficiency will thereafter increase the output power and reduce the bias threshold of lasing significantly.

To further verify whether such an enhancement in lasing performance is induced by piezophototronic effect, another structure (ZnO NWs/MgO/*p*-GaN) with +*c*-axis of the ZnO NWs pointing toward the *p*-GaN has also been fabricated, which is named as LD-b for clarity. The fabrication process of LD-b has been illustrated in Figure S2 (Supporting Information). Similar lasing behaviors have been obtained from LD-b (**Figure 5**), with a threshold voltage of about 43 V. The performances of LD-b under pressure have also been studied, as shown in **Figure 6**. The current of LD-b shows opposite behaviors under pressure, decreasing at positive voltage and increasing at negative voltage, as shown in Figure 6a. Figure 6b shows the decrease of ln*I* and negative equivalent V_{Add} under applied pressure of LD-b. The emission efficiency of LD-b also decreases under pressure, as

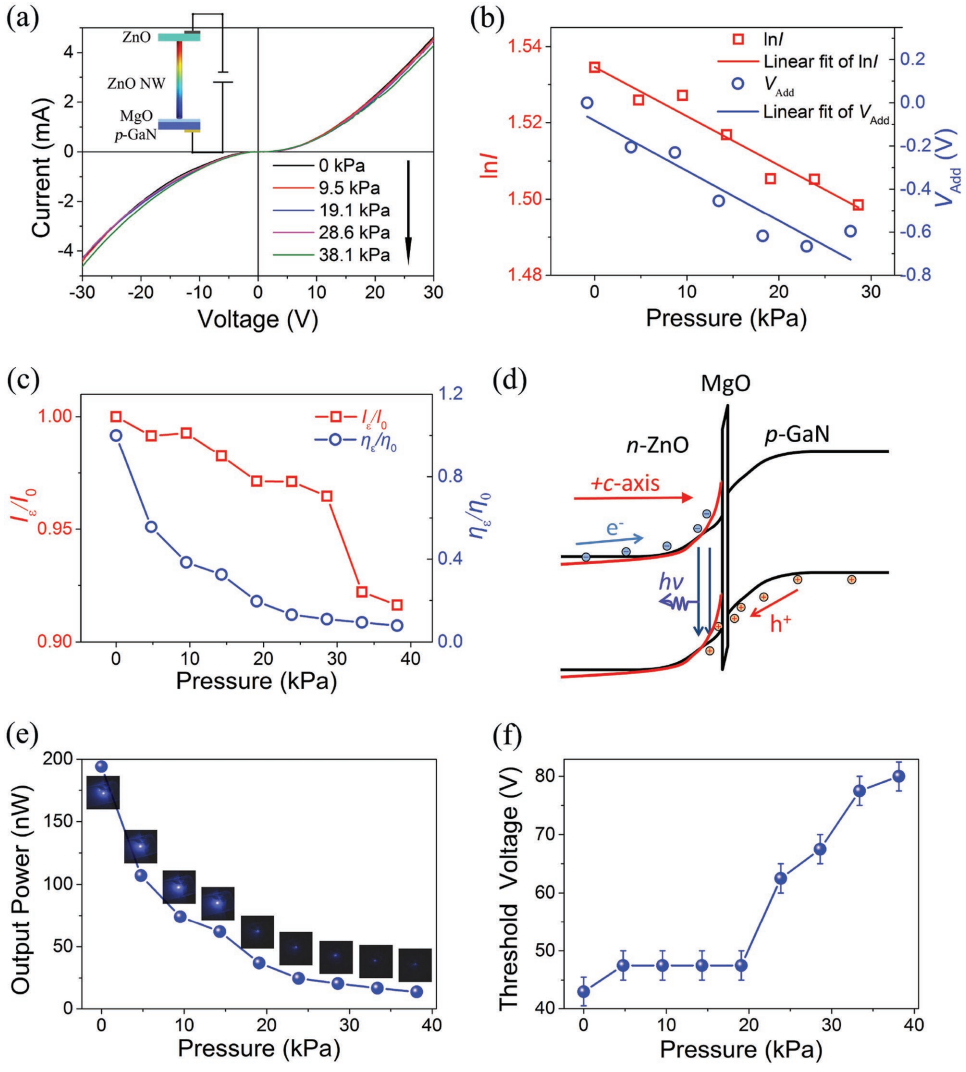

Figure 6. Lasing characteristics of LD-b under pressure. a) *I*–*V* curves as a function of applied pressure and the inset shows the direction of forward bias and piezopotential. b) Logarithm plot of current at a fixed bias of 30 V and the calculated additional external voltage (V_{Add}) versus applied pressure. c) Changes in relative injection current I_ε/I_0 and relative external efficiency η_ε/η_0 under pressure. d) Schematic band diagram of the *p*-GaN/MgO/ZnO NWs before (black line) and after (red line) applying of pressure with *c*-axis of ZnO NWs pointing toward *p*-GaN. e) Decrease of output power and optical images at a fixed bias of 50 V versus pressure. f) Increase of threshold voltage under different pressure.

shown in Figure 6c. In contrary to LD-a, a negative piezopotential is created in the ZnO NWs of LD-b at the *p–n* junction region under pressure. The negative piezopotential in the ZnO NWs may cause the valence and conduction band of the ZnO to bend upward (Figure 6d), which will reduce the density of electrons near the interface of ZnO and MgO, and increase the depletion layer width. The shortage of electrons near the ZnO/MgO interface will lead to a decrease in the recombination rate of electrons and holes. Accordingly, the output power of LD-b at 50 V has been decreased from 194 to 14 nW, and the threshold voltage increased from 43 to 80 V by applying a pressure of 38.1 kPa, as shown in Figure 6e,f. The deteriorated EL performances of LD-b under pressure confirm that the reduced threshold and enhanced emission efficiency observed in LD-a are caused by the piezophototronic effect.

In summary, the piezophototronic effect has been employed to improve the lasing characteristics of semiconductor lasers for the first time. The output power of the laser can be enhanced by a factor of 4.96, and the threshold voltage can be decreased from 48 to 20 V by applying a pressure of 16.0 kPa. The mechanism for the reduced threshold and enhanced emission efficiency can be understood well with the piezophototronic model. The results reported in this paper may be expanded to other polar semiconductors, thus may provide a promising route to enhanced lasing performance of piezoelectric semiconductors; meanwhile, the results may also open another application area for the piezophototronic effect.

Experimental Section

To study the piezophototronic effect on lasers, two *p*-GaN/MgO/ZnO NWs structures with opposite ZnO polarity orientation were fabricated, i.e., LD-a and LD-b. A structural diagram and schematic fabrication process of LD-a are shown in Figure 1a. The *p*-GaN film was grown on *c*-plane sapphire by molecular beam epitaxy (MBE), and the thickness, hole concentration, and Hall mobility of the *p*-GaN are 1.3 μm, 5.3×10^{17} cm^{-3}, and 16.4 cm^2 V^{-1} s^{-1}, respectively. Then a 10 nm MgO film was deposited onto the *p*-GaN film in the MBE system. After that, ZnO NWs were grown on the MgO/*p*-GaN structure via metal-organic chemical vapor deposition (MOCVD) technique. After spin-coating PMMA on the ZnO NWs and exposing the top of ZnO NWs via oxygen plasma, an ITO glass was clipped onto the ZnO NWs to form an electrode. Ni/Au was deposited onto the *p*-GaN by thermal evaporation method acting as another electrode. For LD-a, the +*c*-axis direction of the ZnO NWs is pointing away from *p*-GaN.

For the fabrication of LD-b, ZnO NWs were first grown on sapphire substrate via MOCVD, and then the ZnO NWs were spun coated with PMMA. Meanwhile, *p*-GaN films were grown on sapphire substrate via MBE, and a thin MgO film (10 nm) was deposited onto the GaN layer. After that, the PMMA-coated ZnO NWs and the MgO-coated *p*-GaN were bonded together to form the LD-b, see Figure S1 (Supporting Information). Metallic indium was deposited onto the ZnO NWs as an electrode and Ni/Au deposited onto the *p*-GaN as another electrode. Note that in this case, the +*c*-axis of the ZnO NWs is pointing toward the *p*-GaN, contrary to that of LD-a.

Supporting Information

Supporting Information is available from the Wiley Online Library or from the author.

Acknowledgements

This work was financially supported by the National Science Foundation for Distinguished Young Scholars of China (61425021), the Natural Science Foundation of China (11374296, 11674290, 11134009, and 61376054), and the National Program for Support of Top-notch Young Professionals. The authors would like to thank Prof. Yu Han and Dr. Yihan Zhu from the King Abdullah University of Science and Technology for HRTEM observation and fruitful discussion on the *c*-axis orientation determination with QSTEM simulation.

Received: May 29, 2016
Revised: September 20, 2016
Published online: November 22, 2016

[1] M. H. Huang, S. Mao, H. Feick, H. Q. Yan, Y. Y. Wu, H. Kind, E. Weber, R. Russo, P. D. Yang, *Science* **2001**, *292*, 1897.
[2] X. F. Duan, Y. Huang, R. Agarwal, C. M. Lieber, *Nature* **2003**, *421*, 241.
[3] A. Yamilov, X. Wu, H. Cao, *J. Appl. Phys.* **2005**, *98*, 103102.
[4] X. Wu, A. Yamilov, X. Liu, S. Li, V. P. Dravid, R. P. H. Chang, H. Cao, *Appl. Phys. Lett.* **2004**, *85*, 3657.
[5] R. C. Polson, Z. V. Vardeny, *Appl. Phys. Lett.* **2004**, *85*, 1289.
[6] Q. Song, S. Xiao, Z. Xu, J. Liu, X. Sun, V. Drachev, V. M. Shalaev, O. Akkus, Y. L. Kim, *Opt. Lett.* **2010**, *35*, 1425.
[7] J. Huang, S. Chu, J. Kong, L. Zhang, C. M. Schwarz, G. Wang, L. Chernyak, Z. Chen, J. Liu, *Adv. Opt. Mater.* **2013**, *1*, 179.
[8] X. Y. Liu, C. X. Shan, S. P. Wang, Z. Z. Zhang, D. Z. Shen, *Nanoscale* **2012**, *4*, 2843.
[9] S. Chu, G. Wang, W. Zhou, Y. Lin, L. Chernyak, J. Zhao, J. Kong, L. Li, J. Ren, J. Liu, *Nat. Nanotechnol.* **2011**, *6*, 506.
[10] K. Tang, S. Gu, J. Ye, S. Zhu, R. Zhang, Y. Zheng, *J. Semicond.* **2016**, *37*, 031001.
[11] C. Xu, P. Shin, L. Cao, D. Gao, *J. Phys. Chem. C* **2010**, *114*, 125.
[12] S. Chu, M. Olmedo, Z. Yang, J. Kong, J. Liu, *Appl. Phys. Lett.* **2008**, *93*, 181106.
[13] Z. L. Wang, W. Wu, *Natl. Sci. Rev.* **2013**, *1*, 62.
[14] A. Dalcorso, M. Posternak, R. Resta, A. Baldereschi, *Phys. Rev. B* **1994**, *50*, 10715.
[15] Z. L. Wang, *Adv. Mater.* **2012**, *24*, 4632.
[16] Z. L. Wang, *Nano Today* **2010**, *5*, 512.
[17] Z. L. Wang, J. Song, *Science* **2006**, *312*, 242.
[18] S. N. Cha, J. S. Seo, S. M. Kim, H. J. Kim, Y. J. Park, S. W. Kim, J. M. Kim, *Adv. Mater.* **2010**, *22*, 4726.
[19] J. Zhou, P. Fei, Y. Gu, W. Mai, Y. Gao, R. Yang, G. Bao, Z. L. Wang, *Nano Lett.* **2008**, *8*, 3973.
[20] Y. Yang, J. Qi, Q. Liao, H. Li, Y. Wang, L. Tang, Y. Zhang, *Nanotechnology* **2009**, *20*, 125201.
[21] X. Wang, J. Zhou, J. Song, J. Liu, N. Xu, Z. L. Wang, *Nano Lett.* **2006**, *6*, 2768.
[22] P. Fei, P. H. Yeh, J. Zhou, S. Xu, Y. Gao, J. Song, Y. Gu, Y. Huang, Z. L. Wang, *Nano Lett.* **2009**, *9*, 3435.
[23] Y. F. Hu, Y. Zhang, Y. L. Chang, R. L. Snyder, Z. L. Wang, *ACS Nano* **2010**, *4*, 4220.
[24] F. Boxberg, N. Sondergaard, H. Q. Xu, *Nano Lett.* **2010**, *10*, 1108.
[25] Q. Yang, X. Guo, W. Wang, Y. Zhang, S. Xu, D. H. Lien, Z. L. Wang, *ACS Nano* **2010**, *4*, 6285.
[26] P. Gao, Z. Z. Wang, K. H. Liu, Z. Xu, W. L. Wang, X. D. Bai, E. G. Wang, *J. Mater. Chem.* **2009**, *19*, 1002.
[27] Q. Yang, W. Wang, S. Xu, Z. L. Wang, *Nano Lett.* **2011**, *11*, 4012.

[28] Q. Yang, Y. Liu, C. Pan, J. Chen, X. Wen, Z. L. Wang, *Nano Lett.* **2013**, *13*, 607.
[29] H. Zhu, C.-X. Shan, B. Yao, B.-H. Li, J.-Y. Zhang, Z.-Z. Zhang, D.-X. Zhao, D.-Z. Shen, X.-W. Fan, Y.-M. Lu, Z.-K. Tang, *Adv. Mater.* **2009**, *21*, 1613.
[30] S. J. Jiao, Y. M. Lu, D. Z. Shen, Z. Z. Zhang, B. H. Li, J. Y. Zhang, B. Yao, Y. C. Liu, X. W. Fan, *Phys. Status Solidi C* **2006**, *3*, 972.
[31] S.-K. Hong, T. Hanada, H.-J. Ko, Y. Chen, T. Yao, D. Imai, K. Araki, M. Shinohara, K. Saitoh, M. Terauchi, *Phys. Rev. B* **2002**, *65*, 115331.
[32] X. Yang, C. X. Shan, Y. J. Lu, X. H. Xie, B. H. Li, S. P. Wang, M. M. Jiang, D. Z. Shen, *Opt. Lett.* **2016**, *41*, 685.
[33] C.-S. Wang, C.-H. Nieh, T.-Y. Lin, Y.-F. Chen, *Adv. Funct. Mater.* **2015**, *25*, 4058.
[34] J. H. Choy, E. S. Jang, J. H. Won, J. H. Chung, D. J. Jang, Y. W. Kim, *Adv. Mater.* **2003**, *15*, 1911.
[35] H. D. Li, S. F. Yu, S. P. Lau, E. S. P. Leong, H. Y. Yang, T. P. Chen, A. P. Abiyasa, C. Y. Ng, *Adv. Mater.* **2006**, *18*, 771.
[36] J. Huang, M. M. Morshed, Z. Zuo, J. Liu, *Appl. Phys. Lett.* **2014**, *104*, 131107.
[37] H. Zhu, C. X. Shan, J. Y. Zhang, Z. Z. Zhang, B. H. Li, D. X. Zhao, B. Yao, D. Z. Shen, X. W. Fan, Z. K. Tang, X. Hou, K. L. Choy, *Adv. Mater.* **2010**, *22*, 1877.
[38] Y. Liu, Q. Yang, Y. Zhang, Z. Yang, Z. L. Wang, *Adv. Mater.* **2012**, *24*, 1410.
[39] C. Pan, L. Dong, G. Zhu, S. Niu, R. Yu, Q. Yang, Y. Liu, Z. L. Wang, *Nat. Photonics* **2013**, *7*, 752.
[40] C. Pan, S. Niu, Y. Ding, L. Dong, R. Yu, Y. Liu, G. Zhu, Z. L. Wang, *Nano Lett.* **2012**, *12*, 3302.
[41] W. Shockley, H. J. Queisser, *J. Appl. Phys.* **1961**, *32*, 510.
[42] Y. Gao, Z. L. Wang, *Nano Lett.* **2007**, *7*, 2499.